Draft version September 3, 2022
Preprint typeset using LaTeX style emulateapj v. 04/20/08

arXiv:1010.5238v1 [astro-ph.HE] 25 Oct 2010

INDUCED ROTATION IN 3D SIMULATIONS OF CORE COLLAPSE SUPERNOVAE: IMPLICATIONS FOR PULSAR SPINS

Emmanouela Rantsiou[1], Adam Burrows[1], Jason Nordhaus[1], Ann Almgren[2]

Draft version September 3, 2022

ABSTRACT

It has been suggested that the observed rotation periods of radio pulsars might be induced by a non-axisymmetric spiral-mode instability in the turbulent region behind the stalled supernova bounce shock, even if the progenitor core was not initially rotating. In this paper, using the three-dimensional AMR code CASTRO with a realistic progenitor and equation of state and a simple neutrino heating and cooling scheme, we present a numerical study of the evolution in 3D of the rotational profile of a supernova core from collapse, through bounce and shock stagnation, to delayed explosion. By the end of our simulation ($\sim$420 ms after core bounce), we do not witness any significant spin up of the proto-neutron star core left behind. However, we do see the development before explosion of strong differential rotation in the turbulent gain region between the core and stalled shock. Shells in this region acquire high spin rates that reach $\sim$150 Hz, but this region contains too little mass and angular momentum to translate, even if left behind, into rotational frequencies of significance for the full neutron star. We find also that much of the induced angular momentum is likely to be ejected in the explosion, and moreover that even if the optimal amount of induced angular momentum is retained in the core, the resulting spin period is no faster than $\sim$1.2 seconds, and likely slower.

Subject headings: Hydrodynamics — supernovae: general — pulsars: spin

1. INTRODUCTION

One of the key questions associated with radio pulsars is the origin of their spin periods (Lorimer 2009,2010). In two recent papers (Blondin & Mezzacappa 2007 [hereafter BM07]; Blondin & Shaw 2007), it has been suggested that the growth in 3D of an $\ell = 1$ non-axisymmetric ($m = \{-1, 1\}$) spiral mode (Fernàndez 2010) of the so-called standing accretion shock instability ("SASI") during the post-bounce delay phase seen in current supernova theory can spin up matter in the turbulent region behind the stalled shock. BM07 and Blondin & Shaw (2007) find that the accretion of this spinning matter (and its associated angular momentum) onto the inner core can spin up the nascent neutron star to rotation periods that compare favorably with the observed/inferred values for pulsars at birth. More precisely, they report final periods of $\sim$70 milliseconds (ms) for moderately rotating progenitors and $\sim$50 ms for non-rotating progenitors. The measured period range of birth periods is from $\sim$10 milliseconds to seconds, with an average "injection period" near $\sim$0.5 seconds (Chevalier & Emmering 1986; Narayan 1987)[3]. If this mechanism were to obtain, it would obviate the need to invoke a spinning progenitor core. However, rotation is a natural feature of stars, and there is no obvious reason the progenitor "Chandrasekhar" mass in the center of a massive star at death wouldn't be rotating with the spins and angular momenta needed to leave a compact object with the measured spin frequencies (Ott et al. 2006ab). This is a function of the angular momentum distribution in the cores of massive stars when they collapse (Heger, Woosley, & Spruit 2005; Maeder & Meynet 2000,2004; Hirschi, Meynet, & Maeder 2004). Hence, the possibility that the 3D dynamics of the core itself could generate countervailing flows with opposite signs of angular momentum, "one stream" of which could leave the residue spinning at interesting rates while conserving overall angular momentum, is intriguing. If this were true, to zeroth order all cores at collapse could be non-rotating, and the spins could be a function of collapse dynamics alone. This would eliminate one of the current ambiguities in massive star progenitor models, whose core spins at collapse are not observable. The progenitor cores could all be born with "zero" angular momentum, while giving birth to proto-neutron stars with respectable spins.

However, BM07 and Blondin & Shaw (2007) employed various simplifications in their simulations. They did not follow collapse itself, but started in a steady-state post-bounce configuration. They used a simple "gamma-law" equation of state (EOS), and not a full nuclear EOS. They set the mass accretion rate through the shock to a constant value and did not perform their simulations in the context of a realistic massive-star progenitor. Importantly, they excised the inner core whose very spin-up was being studied. Rather, they inferred from ostensible accretion of matter and angular momentum at their inner boundary an irreversible accumulation of spin in the proto-neutron star. Finally, they did not consider the potential role of the supernova explosion itself on the magnitude of the residual angular momentum and final induced core period. They did, however, investigate the potential role of initial rotation in the final outcome.

In this paper, we investigate the claims of BM07 and Blondin & Shaw (2007), improving upon their study in several ways. Our 3D simulation is described in Nord-

[1] Department of Astrophysical Sciences, Princeton University, Princeton, NJ 08544 USA; emmarant@astro.princeton.edu, burrows@astro.princeton.edu, nordhaus@astro.princeton.edu
[2] Computational Research Division, Lawrence Berkeley National Lab, Berkeley, CA 94720, USA; asalmgren@lbl.gov

[3] The inferred initial spin period of the Crab pulsar is 15−16 milliseconds (Atoyan 1999), but the average for radio pulsars is considerably longer.

haus et al. (2010a) and was carried out using CASTRO (Almgren et al. 2010), an Eulerian Adaptive Mesh Refinement (AMR) hydrodynamics code with hierarchically nested rectangular grids that are refined both in space and time. We employed a realistic EOS (Shen et al. 1998ab) and a simple neutrino transfer scheme (see Nordhaus et al. 2010a and Murphy & Burrows 2008). Both Nordhaus et al. (2010a) and Murphy & Burrows (2008) incorporated the Liebendörfer (2005) prescription for electron capture on infall and a simple neutrino heating and cooling algorithm after bounce. The driving electron and anti-electron neutrino luminosities were kept constant at 1.9×10^{52} ergs s^{-1}. This enabled us to heat the so-called "gain region" (Bethe & Wilson 1985) and investigate the pre-bounce infall, bounce, post-bounce delay, and explosion phases. In this simulation (model 3d:L_1.9 of Nordhaus et al. 2010a), a neutrino-driven explosion occurred approximately $\sim$200$-$250 ms after bounce and we carried the simulation out to $\sim$420 ms after bounce. Our initial model was the 15-$M_\odot$ solar-metallicity, non-rotating red-supergiant model of Woosley & Weaver (1995). An important aspect of our simulation is that the proto-neutron star itself is at all times present on the grid (which is Cartesian) and is followed throughout the run in a hydrodynamically consistent fashion.

The cubic grid in our simulations extended to 10^4 kilometers (km) on each side, with 304^3 cubic cells covering the grid's volume at its coarsest level. Three levels of refinement of a factor of 4 in each dimension were followed. As a result, the resolution in the central regions (the inner 200 km) was $\sim$0.5 km. The monopole approximation for self-gravity was adopted.

By the end of our simulation, we find that there is almost no spin up of the proto-neutron star. During the post-bounce phase and before explosion, the region exterior to the core and interior to the shock ($\sim$60 to $\sim$250 km) does witness the growth of spiral modes, some spin up (to $\sim$150 Hz), and the emergence of countervailing rotational flows. However, the explosion ejects not only mass, but its associated angular momentum, and depending upon where the mass cut is finally imposed, the residual core can end up with some net rotation. In our most optimistic scenario the core achieves a period of only 1.2 seconds. This fastest possible spin does not alone seem adequate to explain the measured and/or inferred pulsar birth periods without significant initial rotation in the progenitor itself. In §2, we present our quantitative results and we follow in §3 with an extended discussion and our summary conclusions.

2. RESULTS

2.1. *Profiles and Temporal Evolution of Angular Momentum*

We begin our analysis by calculating the amount of angular momentum present in our computational domain. We divide the innermost 2000 km of the grid into concentric spheres of increasing radius, and we monitor the magnitude of each of the three components ($x, y,$ and z) of the angular momentum (L_i) enclosed within each sphere for the duration of the calculation after core bounce. The panels in Fig. 1 depict three-dimensional surface representations of the temporal evolution of the three orthogonal components of the total angular momentum enclosed within a certain radius, as a function of that radius. Such panels summarize what we find in our simulation. As Fig. 1 indicates, we do indeed see an initial increase of angular momentum, but only between $\sim$60 km and $\sim$250 km, and quasi-oscillatory behavior with a period near $\sim$30 ms. The innermost zones that might be identified with the proto-neutron star are not spun up to periods faster than $\sim$5$-$10 seconds. At later times (the last 0.17 s after bounce), we note that the angular momentum that originally resided in this inner region is ejected with the exploding mass and follows the outward progress of the reenergized shock. This ejected angular momentum "bump" can also be seen clearly in Fig. 2, where we show the spatial profile of all three components of angular momentum for four different times near the end of our simulation. We address the subsequent fate of this ejected angular momentum in §2.3 and §3. At the end of our simulation, very little angular momentum is left in the central region of our grid, indicating that the inner core is left rotating very slowly. At the final timestep, the spin periods in the inner ten kilometers are all greater than $\sim$10 seconds. Note that the flatness of the regions in Fig. 1 at large distances demonstrates that total angular momentum is very well conserved during the simulation. In CASTRO, angular momentum is not conserved by construction, so that its global conservation during this simulation is encouraging. Specifically, before and after bounce the total angular momentum of matter on the grid is conserved to better than $\sim$1%, staying very near "zero" for the duration of the calculation.

Next, we divide our grid into thin spherical shells that cover the innermost 2000 km of the computational domain. For the inner 250 km the width of the shells was chosen to be 1 km and for radii between 250 and 2000 km the width was increased to 10 km. For each of the shells we calculated the average specific angular momentum (ℓ_i, not the total enclosed angular momentum), for all three components of the angular momentum. Figure 3 depicts their associated spatial and temporal profiles. As discussed above and can be seen in Figs. 1 and 2, regions interior to $\sim$200 km experience some growth of specific angular momentum during the earlier stages after core bounce, whereas the specific angular momentum at larger radii remains close to zero until after the onset of explosion. As Fig. 3 makes clear, the sign of the specific angular momentum for each component varies with time and radius, conserving total angular momentum after bounce to high precision. After the onset of explosion, angular momentum is seen to propagate outward with the ejected mass and the shock wave.

An interesting feature is observed for radii between 60 and 250 km. As time progresses in the simulation, the magnitudes of the specific angular momenta on shells in this region grow with time, indicating that in this region there is indeed some spin up by the spiral mode identified in BM07, Blondin & Shaw (2007), and Fernàndez (2010). We proceed in §2.2 with a discussion of this phenomenon and the associated spin periods.

2.2. *Rotational Period and Frequency Profiles*

Having calculated the angular momentum contained in spherical shells at various radii, we proceed to extract the rotational profiles of those shells. Figure 4 shows the temporal evolution of the average spin frequency (f_i,

in Hz) of each shell, for rotation around the x, y and z axes (the three panels in Fig. 4). We see that shells with radii $R < 60$ km and $R > 250$ km do not develop any significant rotational motion during the entire simulation. However, at the very early times after core bounce and for radii between ∼60 km and ∼250 km in the shocked, turbulent regions, some rotational motion does develop, which with time is amplified. By the end of the simulation, those shells have acquired spin frequencies that reach ∼150 Hz at a radius of ∼100 km, corresponding to a spin period of ∼7 ms. Furthermore, we notice that although at early post-bounce times the sign of the spin vector of those shells kept flipping (as indicated by the positive and negative frequency values shown in Fig. 4), at the end of the simulation neighboring shells tended to align their rotational motion. The left panel of Fig. 5 depicts the velocity field on a ball at radius 90 km near the end of the simulation. As this figure clearly shows, coherent fields of rotation have emerged in this region (see also the panels in Fig. 4). Near the same final time, the shock has been launched into explosion and has the multi-turbule morphology portrayed in the right panel of Fig. 5 as an isoentropy surface.

In Fig. 6 we show the temporal evolution of the magnitude of the specific angular momentum (top) for various shells at different radii, and the corresponding magnitude of the rotational frequency (bottom) of those shells. As in Fig. 4, the development of rotational motion from ∼60 to ∼250 km is obvious and the high spin rate of ∼150 Hz in this narrow range of radii is manifest. However, there is very little mass (∼0.01−0.03 $M_\odot$) and, hence, total angular momentum in this fastest spinning region, and this has major consequences for the spin evolution of the entire residual neutron star.

2.3. *Rotational Periods for the Final State*

Our simulation shows not only that the inner core isn't spun up significantly, but that the mass that does experience an interesting degree of induced rotation is likely to be ejected with the subsequent blast. An interesting question arises associated with this ejected angular momentum "bump," shown in Figs. 1 and 2. If that angular momentum were to be accreted later on onto the central regions (in a "fallback" scenario for angular momentum), what would that imply for the terminal rotation rate of the nascent neutron star? We address this issue by applying various mass cuts to the final state of our simulation. We calculate the total angular momentum enclosed within a given spherical mass cut (given in column 2 of Table 1) and then divide it by a representative moment of inertia for the final-state neutron star (taken to be 2×10^{45} g cm^2 and assuming solid-body rotation) to derive a final angular frequency. Our results are summarized in Fig. 7 and Table 1. For a range of mass cuts between 1.2 and 1.6 $M_\odot$ (baryonic) the final inferred rotational periods vary between 1.2 and 47 seconds (as can be seen in Fig. 7). The fastest inferred period of 1.2 s is seen for a spherical mass cut of 1.53$M_\odot$ baryonic. Note that many measured neutron star masses are near 1.35 $M_\odot$ gravitational, which translates into ∼1.5 $M_\odot$ baryonic.

Apart for the magnitude of such final-state rotational periods, we would also like to know the direction of rotation and how that varies with the different spherical mass cuts. We define two angles to describe the direction of the total angular momentum enclosed within a certain mass cut. Angle θ ($0° \leqslant \theta \leqslant 180°$) is the polar angle, measured with respect to the y-axis, and angle ϕ ($0° \leqslant \phi \leqslant 360°$) is the azimuthal angle, defined with respect to the z-axis. The two last columns of Table 1 show the values of θ and ϕ for the different mass cuts. The direction of the angular momentum varies little for spherical mass cuts from ∼1.2 to ∼1.4 $M_\odot$). However, as Table 1 indicates, it does shows significant variation for mass cuts in the range 1.45 to 1.6 $M_\odot$.

3. DISCUSSION AND CONCLUSIONS

In this paper, we have studied the temporal and spatial evolution of the rotational profile of a newly-formed neutron star. The goal was to test the possibility that the remnant neutron star created in the context of core-collapse supernova could be induced to rotate rapidly due to the growth of a spiral, non-axisymmetric mode of the so-called SASI, even if the progenitor was initially non-rotating. We employed the 3D hydrodynamics code CASTRO to carry out the simulation, starting from the infall phase of a 15-$M_\odot$ non-rotating progenitor, and followed the core bounce, convection, and explosion stages. The core, whose induced rotation was being studied, was included fully on the computational grid, a realistic EOS was used, and a simple neutrino heating and cooling algorithm enabled us to simulate in approximate fashion the turbulent post-bounce delay and subsequent explosive phases. Our main findings are:

- We did not find that a significant spin rate was induced in the nascent neutron star. By the end of our simulation the inner core is seen to rotate very slowly, with spin periods no faster than ∼5−10 seconds.
- However, in the unstable gain region between the shock and the inner core (60 km $< R <$ 250 km), counter-rotating shells can acquire enough specific angular momentum during the stall phase before explosion that they can achieve interestingly high spin rates, reaching frequencies around ∼150 Hz (Fig. 4) and spin periods between ∼6 and ∼100 ms. However, the mass in this region, and the corresponding angular momentum are rather low.
- At the later stages in the evolution of our simulation, the explosion and ejecta transport angular momentum outward behind the exploding shock wave. Even if some of this angular momentum were to fall back at later times, the minimum spin period that the residual neutron star could achieve would be no faster than 1.2 seconds (Fig. 7 and Table 1).

Our results contradict those of BM07, who concluded that enough angular momentum was deposited onto the core to generate spin periods consistent with the observed periods of pulsars, even in the case of non-rotating progenitors. In a recent paper, Wongwathanarat et al. (2010) presented results from a new set of approximate 3D simulations of core-collapse supernovae with non-rotating progenitors. They focused on the remnant neutron star kick velocities (see also Nordhaus et al. 2010b), but also concluded that after ∼1.4 seconds after bounce

TABLE 1
Results at the Final Stage Of The Simulation[(a)]

Spherical Mass Cut (Baryonic) $[M_\odot]$	L $[\times 10^{46}\mathrm{g\ cm^2 s^{-1}}]$	P [s]	f [Hz]	θ $[^o]$	ϕ $[^o]$
1.20	0.501	2.50	0.40	97.6	67.2
1.25	0.531	2.37	0.42	92.1	67.5
1.30	0.479	2.83	0.35	89.7	70.5
1.35	0.380	3.30	0.30	96.7	84.2
1.40	0.252	4.99	0.20	111.6	272.3
1.45	0.125	10.17	0.1	152.5	0.25
1.50	0.619	2.02	0.49	128.6	51.6
1.55	0.790	1.59	0.63	21.6	5.3
1.60	0.027	46.89	0.02	125.5	191.9

[(a)] At $t = 0.422$ s after core bounce; In column 1, we list various spherical mass cuts. The total angular momentum enclosed within that mass is given in column 2. If this enclosed angular momentum were to be left with the nascent neutron star, which we assume to have a moment of inertia of $I \sim 2 \times 10^{45}\mathrm{g\ cm^2}$, then the resulting rotational periods and frequencies would be those presented in columns 3 and 4, respectively. The direction of the total enclosed angular momentum L for each case is represented by two angles given in the last two columns. The polar angle θ ($0^o \leqslant \theta \leqslant 180^o$) is defined with respect to the y-axis and the azimuthal angle ϕ ($0^o \leqslant \phi \leqslant 360^o$) is measured with respect to the z-direction.

the induced spin rates were fairly low, with final periods in the range ∼500 to ∼1000 ms, depending on initial model. Such long periods are qualitatively in accord with those we derive here in our "optimum" case, further challenging the conclusions of BM07.

We emphasize that though our 3D investigation is a significant improvement in all particulars on the studies by BM07 and Blondin & Shaw (207), we handled neutrino physics very approximately. Moreover, we have not explored various progenitor masses, nor a range of initial spin structures. Our goal was to determine whether a sizable rotation rate could be induced in the residual proto-neutron star when the progenitor itself was non-rotating. However, the behavior of the modest spiral mode we do see, and the overall role of rotation in the supernova phenomenon itself, remain to be fully mapped out. As computational capabilities improve, and codes acquire more physics and sophistication, all these issues can and will be readdressed.

The authors would like to acknowledge Rodrigo Fernàndez, Timothy Brandt, John Bell, and Brian Metzger for fruitful discussions and input. A.B. and J.N. are supported by the Scientific Discovery through Advanced Computing (SciDAC) program of the DOE, under grant number DE-FG02-08ER41544. E.R. is supported by the NSF under the subaward no. ND201387 to the Joint Institute for Nuclear Astrophysics (JINA, NSF PHY-0822648), and A.B. receives support from the NSF PetaApps program, under award OCI-0905046 via a subaward no. 44592 from Louisiana State University to Princeton University. Work at LBNL was supported in part by the SciDAC Program under contract DE-AC02-05CH11231. The authors would like to thank the members of the Center for Computational Sciences and Engineering (CCSE) at LBNL for their invaluable support for CASTRO. The authors employed computational resources provided by the TIGRESS high performance computer center at Princeton University, which is jointly supported by the Princeton Institute for Computational Science and Engineering (PICSciE) and the Princeton University Office of Information Technology; by the National Energy Research Scientific Computing Center (NERSC), which is supported by the Office of Science of the US Department of Energy under contract DE-AC03-76SF00098 and on the Kraken and Ranger supercomputers, hosted at NICS and TACC and provided by the National Science Foundation through the TeraGrid Advanced Support Program under grant number TGAST100001.

REFERENCES

Almgren, A.S., Beckner, V.E., Bell, J.B., Day, M.S., Howell, L.H., Joggerst, C.C., Lijewski, M.J., Nonaka, A., Singer, M., & Zingale, M. 2010, ApJ, 715, 1221
Atoyan, B. M. 1999, A&A, 346, L49
Blondin, J. M., & Mezzacappa, A. 2007, Nature, 445, 58
Blondin, J. M., & Shaw, S. 2007, ApJ, 656, 366
Chevalier, R. & Emmering, R.T. 1986, ApJ, 304, 140
Fernàndez, R. 2010, arXiv:1003.1730
Heger, A., Woosley, S. E., & Spruit, H. C. 2005, ApJ, 626, 350
Hirschi, R., Meynet, G., & Maeder, A. 2004, A&A, 425, 649
Liebendörfer, M. 2005, ApJ, 633, 1042
Lorimer, D. R. 2009, Astrophys. & Space Sci. Lib., 357, 1
Lorimer, D. R. 2010, to appear in the Proceedings of the ICREA Workshop on The High-Energy Emission from Pulsars and their Systems, held in Sant Cugat, Spain, 2010 April 12-16 (Springer), arXiv:1008.1928
Maeder, A. & Meynet, G. 2000, ARA&A, 38, 143
Maeder, A. & Meynet, G. 2004, A&A, 422, 225
Murphy, J. W., & Burrows, A. 2008, ApJ, 688, 1159
Narayan, R. 1987, ApJ, 319, 162
Nordhaus, J., Burrows, A., Almgren, A., & Bell, J. 2010a, ApJ, 720, 694
Nordhaus, J., Brandt, T., Burrows, A., Livne, E. & Ott, C.D. 2010b, submitted to Phys. Rev. D, arXiv:1010.0674
Ott, C. D., Burrows, A., Thompson, T. A., Livne, E., & Walder, R. 2006a, ApJS, 164, 130
Ott, C. D., Burrows, A., Livne, E., & Walder, R. 2006b, ApJ, 600, 834
Shen, H., Toki, H., Oyamatsu, K., & Sumiyoshi, K. 1998a, Nucl. Phys. A, 637, 435
—. 1998b, Prog. Th. Phys., 100, 1013
Wongwathanarat, A., Janka, H.-Th. & Müller, E. 2010, submitted to ApJ, arXiv:1010.0167
Woosley, S. E. & Weaver, T. A. 1995, ApJS, 101, 181

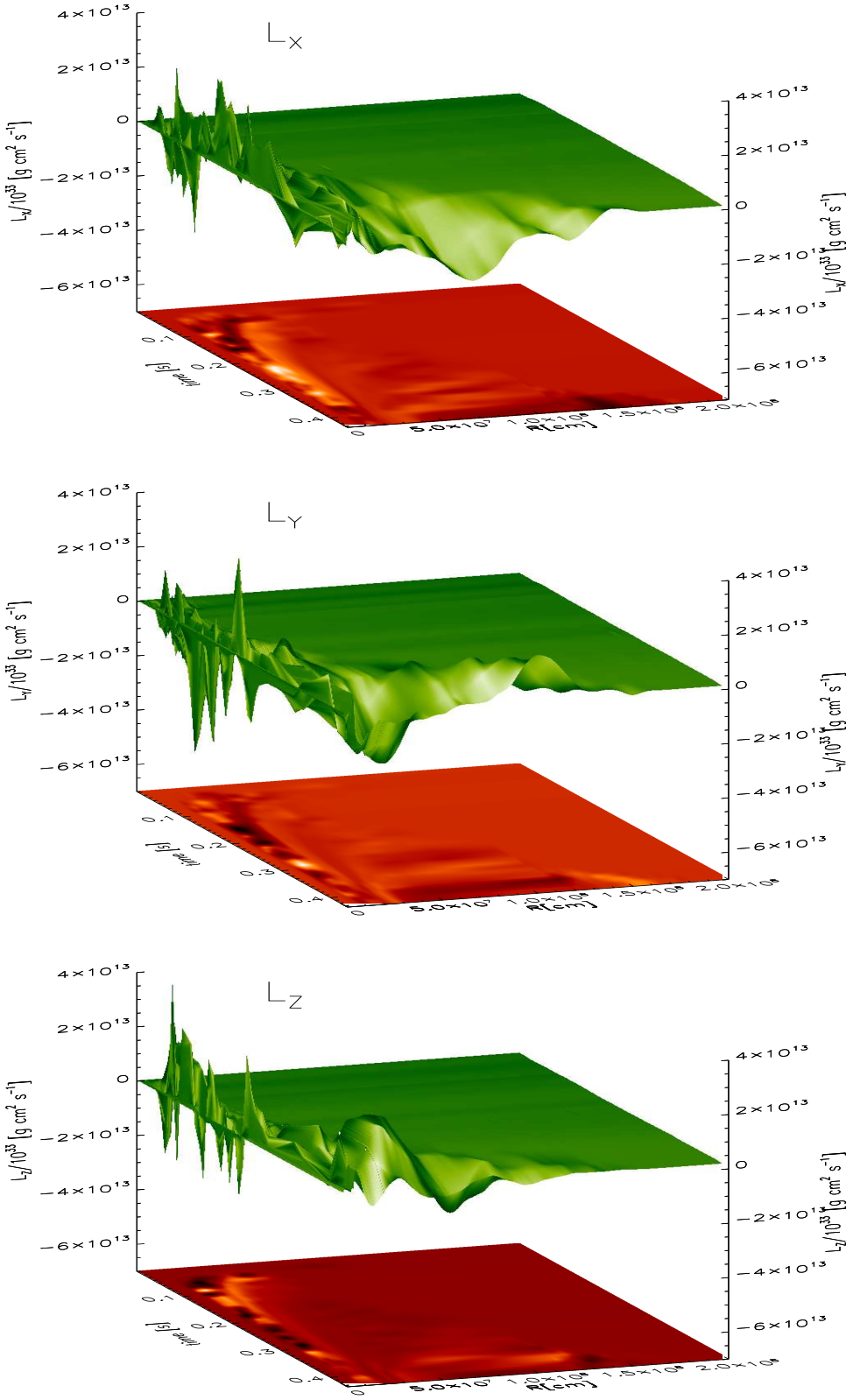

FIG. 1.— Three-dimensional surface representation of the temporal evolution (after bounce) of the components (L_i) of the total angular momentum (vertical axes) enclosed within a spherical radius R (in km). The three panels, from top to bottom, correspond to the x-, y-, and z-components of the enclosed angular momentum. The two-dimensional plot under each surface shows the projection of the upper surface onto the plane, with the color variation indicating the value of the projected point, going from black (negative) to white (positive) through a scale of red shades. We notice the initial increase of the angular momentum components in the very inner regions of our computational domain, and the ejection (with the ejected mass) of the bulk of angular momentum outwards during the later stages of the simulation. See text in §2.1 for further discussion.

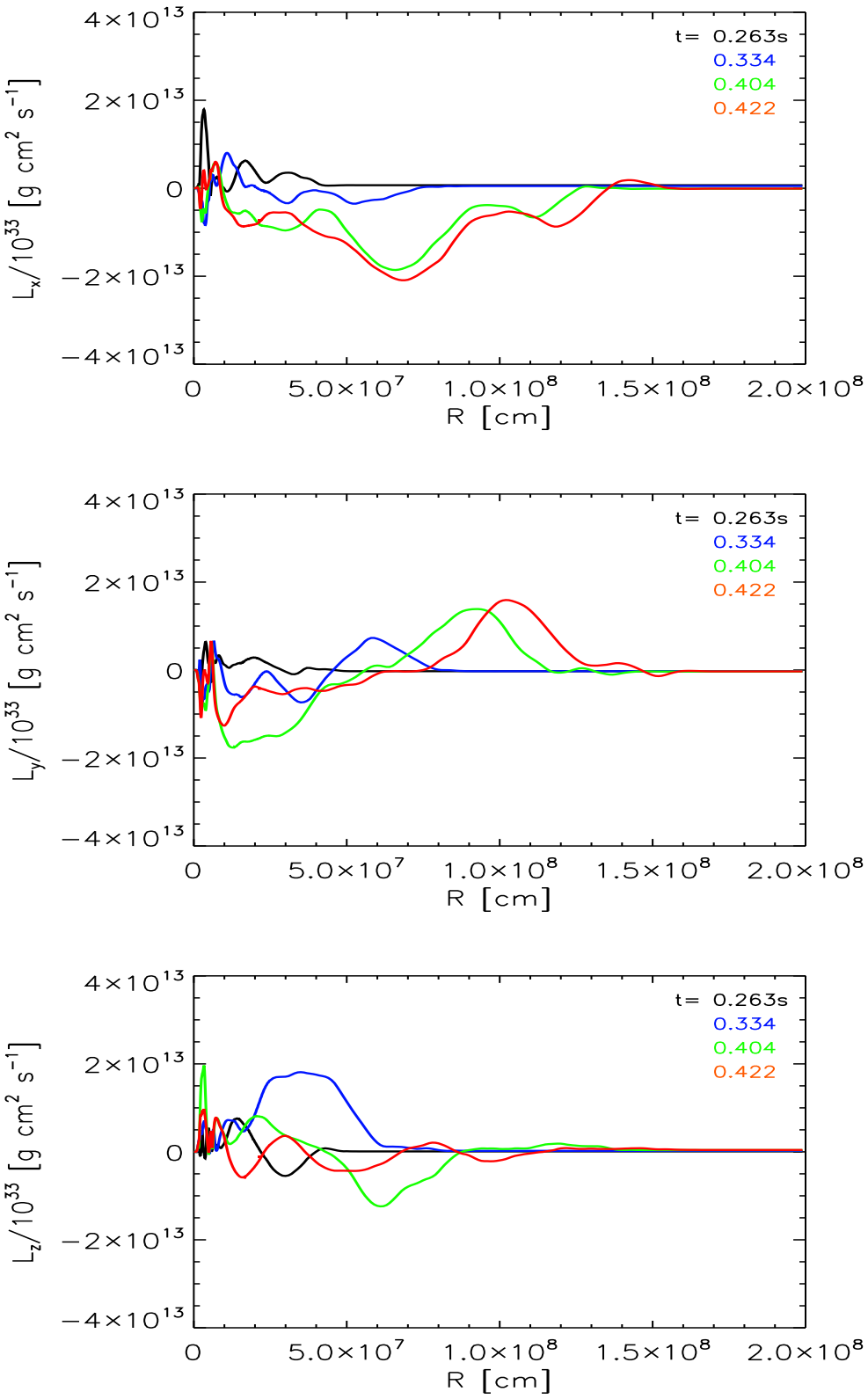

FIG. 2.— Total angular momentum enclosed within a spherical radius R and its evolution with time after bounce, for four different timesteps. The three panels correspond to the three components of the angular momentum vector (x, y and z components from top to bottom, respectively). Lines of different color indicate different post-bounce times during the simulation. We notice again (as in Fig. 1) an initial increase of the angular momentum components between ∼60 and ∼200 km. With time, much of the angular momentum is ejected with the exploding mass. This can be seen here in the propagating angular momentum "bump." As discussed in the text and also in the captions to Table 1 and Fig. 7, this ejected angular momentum, if actually all accreted onto the neutron star at later time, would induce a rotational period no faster than 1.2 s.

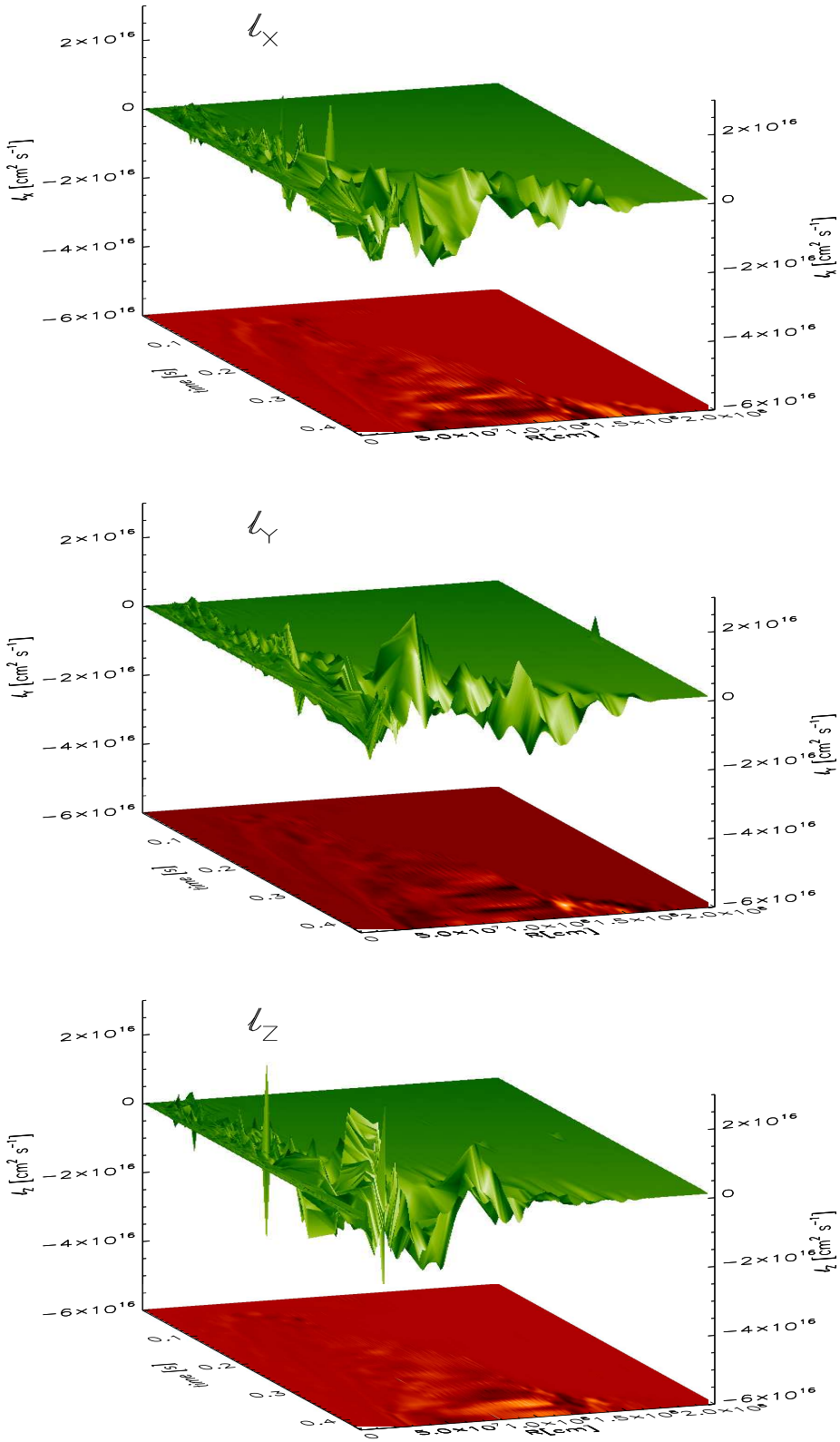

FIG. 3.— Temporal evolution (in seconds after bounce) of the average specific angular momentum (ℓ_i, vertical axes) of spherical shells at various enclosed spherical radii (R, in centimeters). R is logaritmically distributed. From top to bottom, the three panels correspond to the x-, y-, and z-component of the specific angular momentum. To determine the averages, the computational grid was divided into thin spherical shells of width 1 km within the inner 250 km of the grid and of width 10 km for radii between 250 and 2000 km. The two-dimensional surfaces under each upper surface are projections of the upper surfaces, with the color variation indicating the value of the projected point, going from black (negative) to white (positive) through a scale of ɡ shades. The propagation outward at later times of the induced angular momentum is manifest in these panels as well. See the text in §2.1 for a discussion.

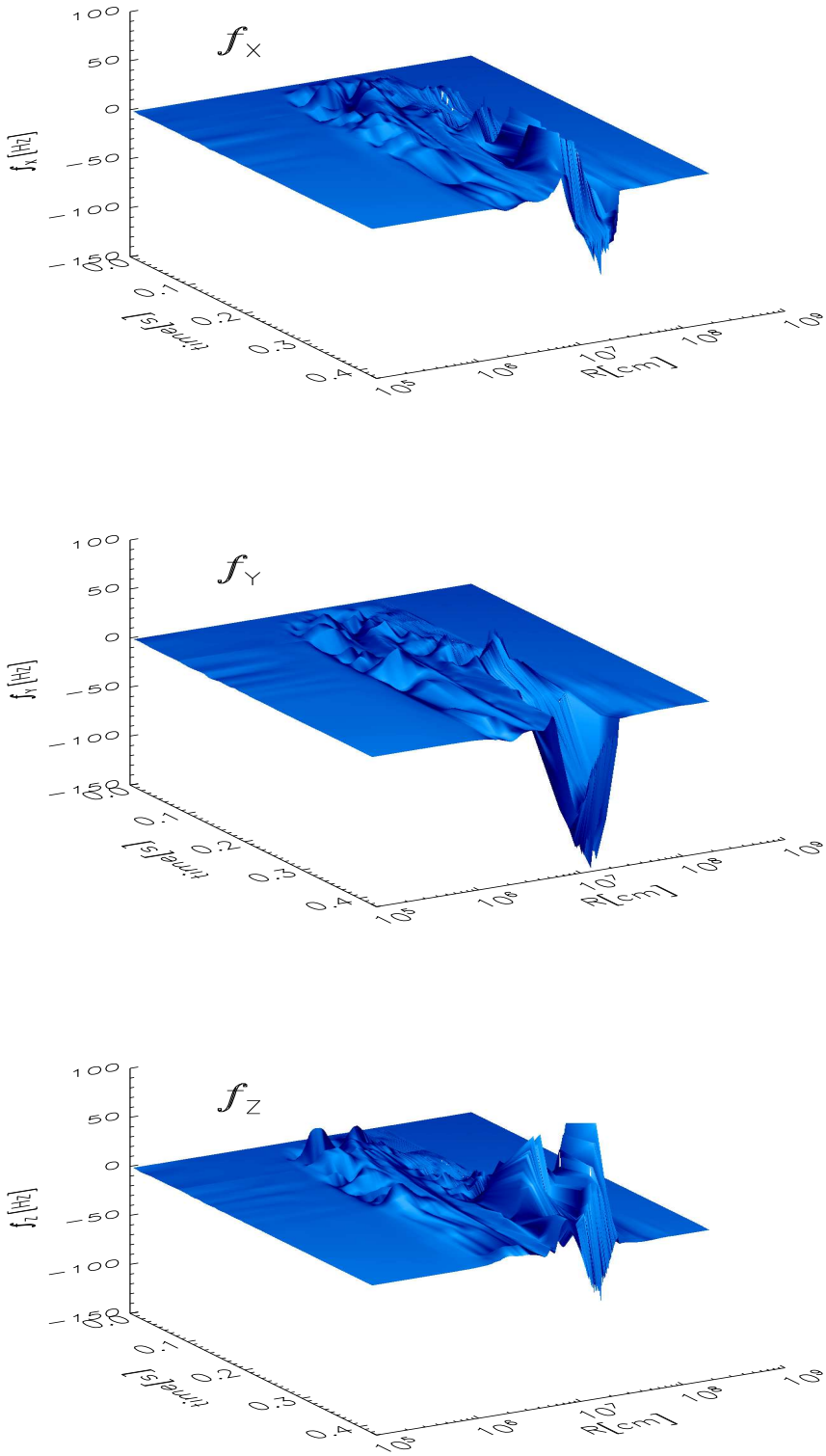

FIG. 4.— The temporal evolution of the spin frequency profiles of thin spherical shells at various spherical radii R (in centimeters, shown logarithmically). For each of the individual shells we have calculated the corresponding average rotational frequency, shown here on the vertical axis of each plot. Time is the post-bounce time in seconds. The three panels correspond to rotation around the x, y and z axes (from top to bottom). The positive and negative values of the frequency indicate opposite rotation directions. The computational grid was divided into thin spherical shells of width 1 km within the inner 250 km of the grid and of width 10 km for radii between 250 and 2000 km. We notice that for radii in the range $R < 60$ km and $R > 250$ km, the resulting frequencies remain near "zero" throughout the entire simulation. Interestingly, in the region $60 < R < 250$ km, some rotational motion develops even during the early stages of the simulation and amplifies during the very late stages, producing shell rotational frequencies that reach ∼150 Hz at a radius of 100 km. See text in §2.2 for a discussion.

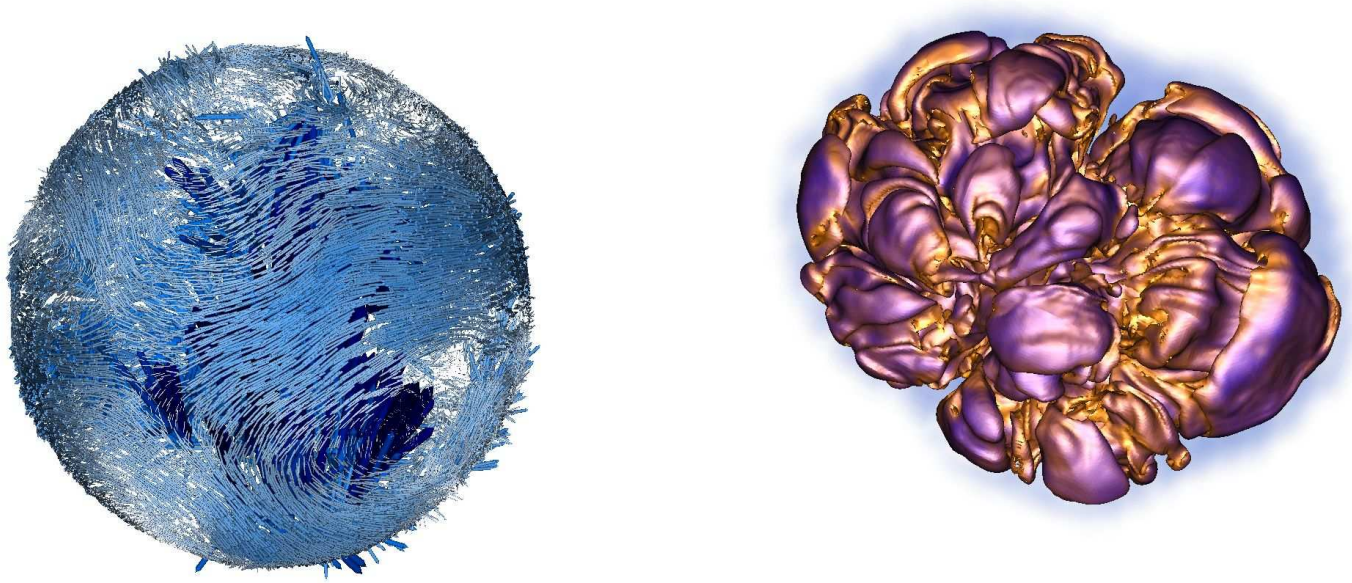

FIG. 5.— **Left:** Velocity vector field profile on a spherical shell of radius 90 km towards the end of the simulation (∼370 ms after core bounce). Both the size and color of the vectors represent the magnitude of the velocity field, with darker (lighter) shades corresponding to higher (lower) values. **Right:** 3D rendering of an isentropic surface with entropy equal to 10 k_b baryon^{-1}. The colormap represents the magnitude of the entropy gradient on the surface, with values increasing going from orange to purple. The surface spans 1600 km and corresponds to a time 380 ms after core bounce.

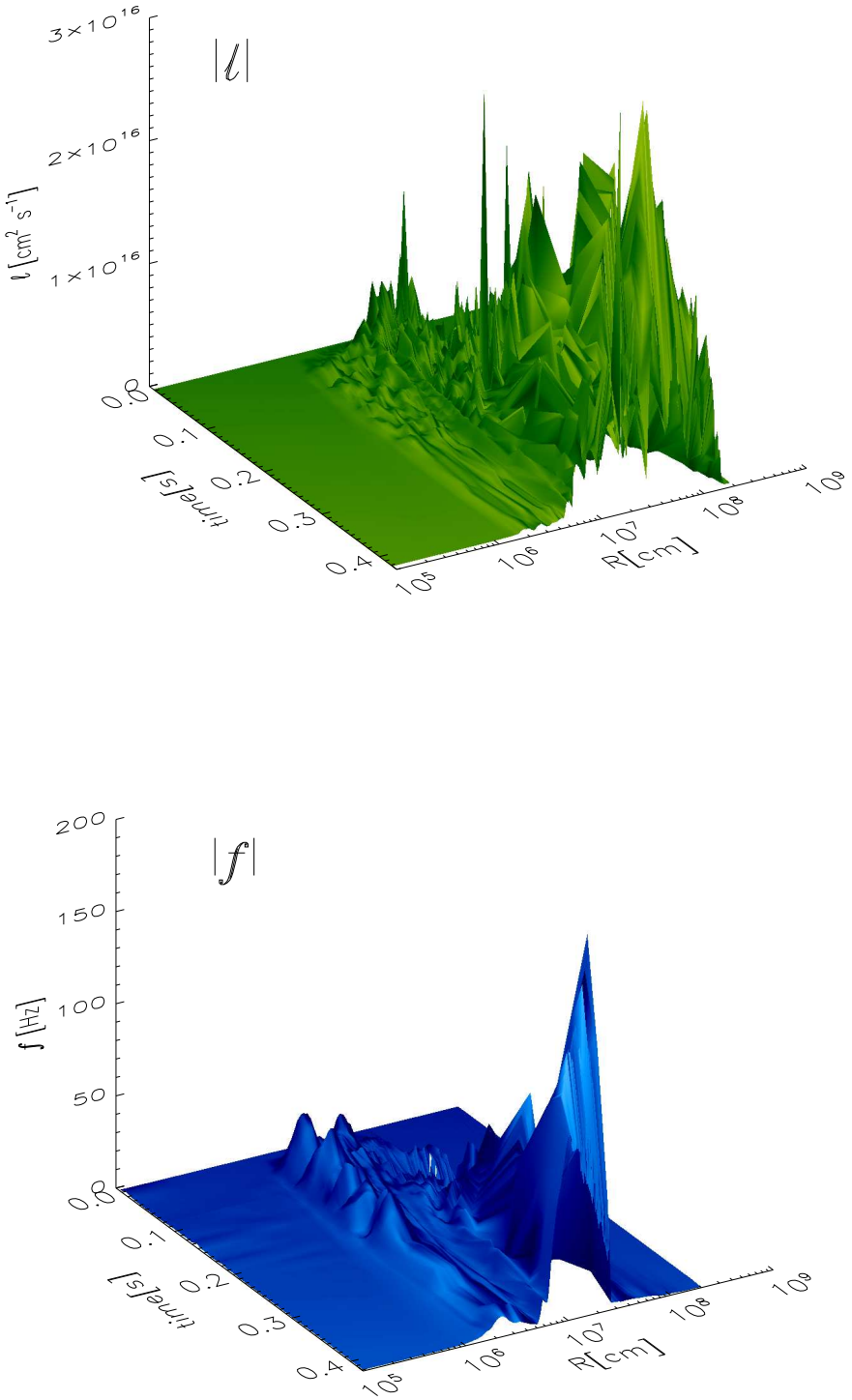

FIG. 6.— Temporal evolution (in seconds) of the magnitude of the specific angular momentum (top) and of the magnitude of the rotational frequency (bottom) of spherical shells at various spherical radii R (in centimeters, shown logarithmically). As discussed in the caption to Fig. 4 and in the text, individual shells at radii $60 < R < 250$ km develop significant rotational frequencies over time. However, outside this range of radii the rotation induced by non-axisymmetric instabilities is quite modest at all times during the simulation.

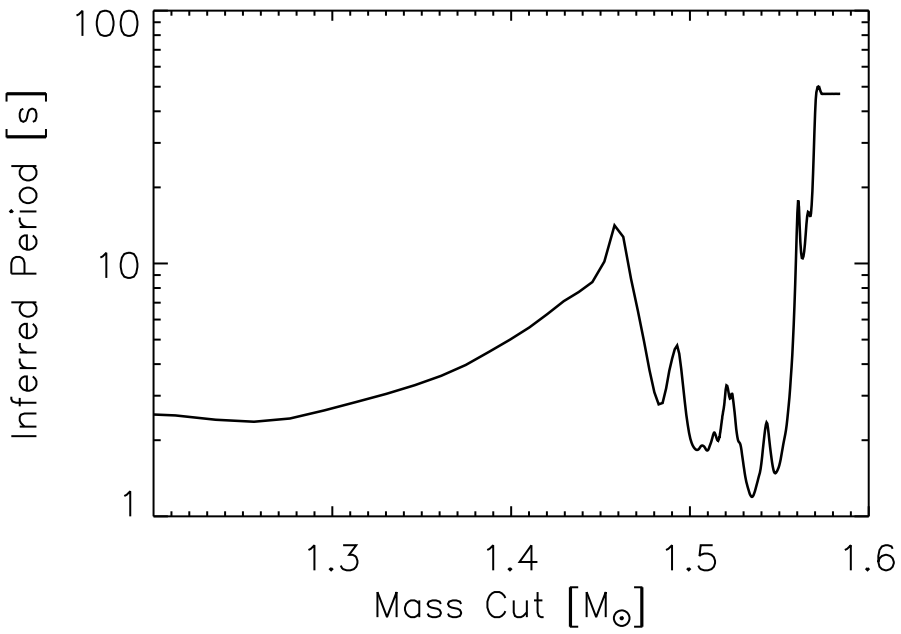

FIG. 7.— Rotation periods of inferred final-state neutron stars as a function of various possible mass cuts (in $M_\odot$), as described in the caption to Table 1 and in the text. To derive these approximate final spin periods, the enclosed total angular momentum is divided by a final neutron star moment of inertia of 2×10^{45} g cm^2. Solid-body rotation for the final state is assumed. The fastest induced spin up is seen to be for a mass cut of 1.53 $M_\odot$ (baryonic mass), resulting in a slow rotational period of $\sim$1.2 seconds.